UNIVERSITY OF LEEDS

This is a repository copy of *Microstructure and Nanoscaled Characterization of HVFA Cement Paste Containing Nano-SiO_2 and Nano-$CaCO_3$*.

White Rose Research Online URL for this paper:
https://eprints.whiterose.ac.uk/141610/

Version: Accepted Version

Article:
Shaikh, FUA, Supit, SWM and Barbhuiya, S (2017) Microstructure and Nanoscaled Characterization of HVFA Cement Paste Containing Nano-SiO_2 and Nano-$CaCO_3$. Journal of Materials in Civil Engineering, 29 (8). ARTN 04017063. ISSN 0899-1561

https://doi.org/10.1061/(ASCE)MT.1943-5533.0001898

© 2017 American Society of Civil Engineers. This material may be downloaded for personal use only. Any other use requires prior permission of the American Society of Civil Engineers. This material may be found at https://doi.org/10.1061/(ASCE)MT.1943-5533.0001898.

Reuse
Items deposited in White Rose Research Online are protected by copyright, with all rights reserved unless indicated otherwise. They may be downloaded and/or printed for private study, or other acts as permitted by national copyright laws. The publisher or other rights holders may allow further reproduction and re-use of the full text version. This is indicated by the licence information on the White Rose Research Online record for the item.

Takedown
If you consider content in White Rose Research Online to be in breach of UK law, please notify us by emailing eprints@whiterose.ac.uk including the URL of the record and the reason for the withdrawal request.

White Rose university consortium
Universities of Leeds, Sheffield & York

eprints@whiterose.ac.uk
https://eprints.whiterose.ac.uk/

Microstructure and nanoscaled characterisation of HVFA cement paste containing nano-SiO_2 and nano-$CaCO_3$

Faiz U. A. Shaikh*,

Senior Lecturer, Department of Civil Engineering, Curtin University, Perth, Australia.

Steve W.M. Supit

Former PhD student, Department of Civil Engineering, Curtin University, Perth, Australia.

Salim Barbhuiya

Lecturer, Department of Civil Engineering, Curtin University, Perth, Australia.

*Corresponding author (s.ahmed@curtin.edu.au)

ABSTRACT

This paper presents the effects of nano-SiO_2 and nano-$CaCO_3$ on the microstructure of High Volume Fly Ash (HVFA) cement paste. The microstructure of HVFA cement paste containing 40% and 60% class F fly ash were evaluated at 28 days using nanoindentation, X-ray diffraction (XRD), thermogravimetric (DTA/TGA) and mercury intrusion porosimetry (MIP) analysis. There was a reduction of calcium hydroxide (CH) in XRD analysis of HVFA pastes containing nanoparticles. This observation was also confirmed in the DTA/TGA analysis. The nanoindentation results also showed the evidence of pozzolanic reaction in the HVFA pastes where the addition of 2% nano-SiO_2 and 1% nano-$CaCO_3$ increased the volume fractions of high-density and low-density calcium-silicate-hydrate (CSH) gels and confirmed the ability of nanoparticles in reducing the porosity of HVFA pastes, which was in consistent with the MIP analysis. The improved nano and microstructure of HVFA pastes due to the addition of nano-SiO_2 and nano-$CaCO_3$ obtained in this study show that high strength and highly durable sustainable concrete can be produced with less repair and maintenance requirements of the concrete structures.

Keywords: High volume fly ash, nano-SiO_2, nano-$CaCO_3$, microstructure, nanoindentation, porosity.

1. Introduction

Fly ash, a by-product of coal-fired power station, has long been used as a partial replacement of ordinary Portland cement (OPC) in concrete production. It acts as a pozzolanic material, which reacts with Calcium Hydroxide (CH), a product of cement hydration and forms additional Calcium Silicate Hydrate (C-S-H) and Calcium Aluminate Hydrate (C-A-H) phases. These effectively contribute to higher strength and better durability of concrete through the formation of dense microstructure (Tahir and Sabir, 2005, Malvar and Lenke, 2006, Bendapudi, 2011). In view of sustainability of concrete, it is desirable to use fly ash in large quantities (Malhotra and Mehta, 2002). In many research the replacement of OPC by 50% or more fly ash is termed as high volume fly ash replacement (Siddique, 2004; Malhotra and Mehta, 2002). Previous studies have shown that the partial replacement of OPC by high volume fly ash improved the workability of concrete (Malhotra and Mehta, 2002). However, the early age mechanical and durability properties of HVFA concrete is inferior to the OPC concrete (Siddique, 2004). To overcome this limitation, various pozzolanic materials such as silica fume, ultrafine fly ash, fine lime powder, slag, etc. have been used in concrete (Mehta,

2004; Shi and Shao, 2002; Pera et al., 1999; De Weerdt, 2011; Supit et al., 2014; Shaikh and Supit, 2015). Due to their smaller particle size and higher surface area than the fly ash, the low compressive strength of HVFA concrete at early age is improved.

The use of nanomaterials to improve various properties of concrete is relatively new in concrete technology and has received particular interest among researchers in recent years (Sato and Beaudoin, 2011; Shaikh and Supit, 2014; Supit and Shaikh, 2014a,b; Hou et al., 2013; Li et al., 2004; Shaikh et al., 2014). Among various nanomaterials the beneficial effects of using nano-SiO_2 and nano-$CaCO_3$ on the mechanical and durability properties of HVFA cement paste system is reported in a number of studies (Hou et al., 2013; Li et al., 2004; Sato and Beaudoin, 2011) including authors recent studies (Shaikh and Supit, 2014; Supit and Shaikh, 2014a,b; Shaikh et al., 2014). It was found that both the early-age and the long-term compressive strength and durability properties of HVFA concretes are significantly improved due to the addition of nano-SiO_2 and nano-$CaCO_3$. The formation of dense microstructure in HVFA concrete due to the addition of these nanoparticles was found to be the main reason for the superior properties.

While the addition of nanomaterials in HVFA concretes showed significant improvement in strength and durability properties very few studies reported their effect on the microstructure of HVFA cement paste. Hou et al. (2013) studied the microstructure of fly ash cement paste containing colloidal nano-SiO_2 using scanning electron microscopy (SEM) technique. The SEM examination showed double layer coating structure in the nano-SiO_2 added high volume fly ash paste, which after closer examination revealed to be compact layer structure. Kawashima et al. (2014) studied the microstructure of 30% fly ash cement paste with 2.5% and 5% nano-$CaCO_3$ under the SEM and reported no noticeable difference between the microstructure of fly ash cement paste and that containing nano-$CaCO_3$, although compressive strength at 2.5% nano-$CaCO_3$ was higher than the control paste. Recently, nanoindentation technique was used for nanoscaled characterisation of different hydration phases e.g. C-S-H, CH, ettringite, etc. of cement paste matrix through measuring the stiffness of individual phases (Sorelli et al., 2008; Constantinides, and Ulm, 2004; Vandamme et al., 2010, Zhou et al., 2007). No study so far reported different hydration phases identification of high volume fly ash cement paste containing nano-SiO_2 and nano-$CaCO_3$ using this technique. This paper reports the microstructure and nanoscaled characterisation of HVFA cement paste containing nano-SiO_2 and nano-$CaCO_3$ using nanoindentation, X-ray diffraction (XRD), thermogravematry (DTA/TGAA) and Mercury Intrusion Porosimetry (MIP) analysis.

2. Experimental programme

2.1 Materials and mix proportions

Ordinary Portland cement Type I (PC), Class F fly ash (FA), nano-SiO_2 and nano-$CaCO_3$ were used in this study. The nano-SiO_2 and nano-$CaCO_3$ were white powder with an average particle diameter of 25 nm and 40-50 nm, respectively. Nano-SiO_2 was obtained from Nanostructured and Amorphous Materials, Inc. of USA whereas nano-$CaCO_3$ was obtained from Skyspring nanomaterials Inc. of USA. The chemical analysis and physical properties of all materials used are listed in Table 1. In total six mixes of HVFA cement paste were cast. The first two mixes were control HVFA cement pastes containing 40% and 60% class F fly ash. In third and fourth mixes 2% nano-SiO_2 was added while in fifth and sixth mixes 1% nano-$CaCO_3$ was added. The selected quantities of nano-SiO_2 and nano-$CaCO_3$ were based on author's recent studies (Shaikh and Supit, 2014; Supit and Shaikh, 2014a,b; Shaikh et al., 2014). Details of mix proportions of all mixes are shown in Table 2. The nano-SiO_2 and nano-$CaCO_3$ were dry mixed with fly ash and cement in a Hobart mixer for 3–4 min followed by the addition of water and wet mixed for an additional 2–3 min.

2.2 Test methods

In order to study the microstructure and the nanoscaled behaviour of HVFA pastes, 50mm cubes were cast and demolded after 24 hours. The paste specimens were cured in water at room temperature for 28 days. Small samples were cut from the cubes to perform the nanoindentation, XRD, DTA/TGA and MIP. The small cut paste samples for nanoindentation tests were polished using silicon carbide paper. The polishing was done using a finer abrasion of silica carbide (9 μm, 6 μm, 3 μm, 1 μm, 0.25 μm and 0.1 μm) for 40 minutes each with their respective diamond suspension fluid.

2.2.1 Nanoindentation

In nanoindentation, a controlled load was applied on the surface of materials in order to induce a local deformation. Using well-established equations, which are based on the principles of elastic contact theory, reduced elastic modulus and hardness were calculated. The applied load and the corresponding displacement were continuously monitored during the test. This resulted in a load-displacement curve as shown in Fig. 1. The slope at the beginning of the unloading curve is defined as the contact stiffness (S), and is given by:

$$S = \frac{dP}{dh} \text{-------- (1)}$$

where P is the indentation load and h is the indentation depth.

The initial part of the unloading curve is fitted by a Power Law:

$$S = \frac{2}{\sqrt{\ }} \frac{1}{E_r} \div \sqrt{A_c} \quad \text{-------- (2)}$$

where E_r is the reduced modulus, A_c is the contact area of the indenter and β is a constant for the indenter geometry.

E_r is related to the elastic modulus of the sample (E) and the elastic modulus of the indenter (E_i) by the following equation:

$$\frac{1}{E_r} = \frac{1}{E} + \frac{1}{E_i} \quad \text{------- (3)}$$

where v is the Poisson's ratio of the sample and v_i is the Poisson's ratio of the indenter. For the Berkovich indenter, the E_i and v_i are 1140 GPa and 0.07 respectively. Therefore, the reduced elastic modulus, E_r, can be defined as:

$$E_r = \frac{\sqrt{\ }}{2} \frac{S}{\sqrt{A_c}} \quad \text{-------- (4)}$$

The hardness is defined by:

$$H = \frac{P_{\max}}{A_c} \quad \text{-------- (5)}$$

where P_{max} is the peak load.

The nanoindentation machine used in this study was an Agilent Nano Indenter® G200 fitted with a Berkovich indenter tip of size 20nm. The calibrated contact area function was derived from indentation tests conducted previously on a fused quartz standard specimen. All testing were programmed in such a way that the loading started when the indenter came into contact with the test surface. The load was maintained for 30 seconds at the pre-specified maximum value before unloading. The unloading data for the lower indentation depth (i.e. h_p = 300–400 nm) was used to determine the reduced modulus and hardness values of the indentation point. A typical micrograph showing indents is shown in Fig. 2.

Information on the mechanical properties was obtained from a matrix of 320 indents on the surface for cement composite samples. The selected indent spacing was 20 μm. Grid indentation technique was used to ensure that a representative set of data was collected for the

samples. The selected method of grid indentation was 4x10 indents per area. On each sample this was repeated 8 times for a total of 320 indentation tests per sample. Each test area was selected by manual inspection using the indenters built in microscope.

The nanomechanical properties of specific individual phases were extracted by statistically analysing all the test results, using a method similar to that presented by Constantinides et al., 2003. Basically, the experimental data (i.e. modulus and hardness values) were statistically analysed to produce a frequency histogram. Then, the best model fit to the experimental results with multimodal normal distribution curves (also known as Gaussian distribution, Eq. 1 was produced using nonlinear least squares method.

$$f(x, \quad , \quad) = \frac{1}{\sqrt{2}} \exp \quad \frac{(x \quad)^2}{2 \quad ^2} \div \qquad (6)$$

From each model fit, the mean value μ and standard deviation σ of the distribution were extracted. The area under the normal distribution curve also provides an estimate of the volume fraction for the hydrate/mineral phase it associated with, within the area of the sample covered by indents.

2.2.2 X-ray diffraction (XRD)

The powder of paste samples (3 g) were used for XRD analysis. The samples were milled using a ring mill (Rocklabs Ltd., New Zealand) with a tungsten carbide head to get a fine powder sample (particle size about 75 microns), before packing them into holders. The sample was milled for 30 seconds. XRD patterns were acquired on a Siemens D500 Bragg-Brentano Diffractometer (Munich, Germany). Operating conditions were set a 40 kV and 30 mA using a Cu$k\alpha$ X-ray source. An analysis from 5^0 to 70^0 (2θ) is carried out at a speed of 0.5^0/min.

2.2.3 Thermal analysis (DTA/TGA)

DTA/TGA analysis measures both heat flow and weight changes in a material as a function of temperature and time in a controlled atmosphere. DTA curves show the thermal decompositions of different phases in paste, while TGA simultaneously measures the weight loss due to the decomposition of phases. About 50 mg of well-powdered sample in a 110 μL platinum crucible was heated from ambient to 1000°C at 20°C per minute in a nitrogen atmosphere flowing at 100 ml per minute. Mass and differential temperature data were

acquired with respect to furnace temperature. The analysis also allows the estimation of the content of CH from the weight losses in paste samples. The calcium hydroxide (CH) content can be calculated according to Taylor formula (1990):

$$CH(\%) = WL_{CH}(\%)\frac{MW_{CH}}{MW_{H_2O}} \text{------} \qquad (7)$$

Where:

WL_{CH} is the weight loss during the dehydration of CH as percentage of the ignited weight (%)

MW_{CH} is the molecular weight of CH

MW_{HO} is the molecular weight of H_2O

2.2.4 Mercury intrusion porosimetry (MIP)

The mercury intrusion porosimetry (MIP) test was performed to measure the pore volumes and their distribution in the HVFA pastes containing nanoparticles. This measurement was performed with a PoreMaster series - Quantachrome instruments, with a pressure ranged between 0.0083 and 207 MPa, and the pore diameter and intrusion mercury volume were recorded at each pressure point. The pressures were converted to equivalent pore diameter using the Washburn equation, as expressed in Equation (8):

$$d = \frac{4 \ \cos}{P} \text{ ------- } (8)$$

Where d is the pore diameter (µm), γ is the surface tension (mN/m), θ is the contact angle between mercury and the pore wall (°), and P is the net pressure across the mercury meniscus at the time of the cumulative intrusion measurement (MPa).

3. Results and discussion

3.1 Nanoindentation analysis

In this study, the indentation modulus frequency distribution was used to obtain different phases (Loose-pack CSH, Outer (Low Density) CSH, Inner (High Density) CSH, and CH) of HVFA cement pastes. These phases are denoted as model 1, model 2, model 3 and model 4, respectively in Figs. 3-8, where the probability distribution of indentation modulus and hardness of HVFA pastes measured after 28 days of curing is presented. The bin width used for Young's modulus was 2.2 whereas this was 0.075 for hardness. The ranges of values of modulus that were used in the creation of the models have been taken from existing literature as ≤10±2, 11±2 - 24±2, 29±2 - 33±2 and 35±2 – 50 GPa for Loose-pack CSH, Outer (Low Density) CSH, Inner (High Density) CSH, and CH, respectively (Sorelli et al., 2008;

Constantinides, and Ulm, 2004; Vandamme et al., 2010, Zhou et al., 2007). The values of elastic modulus higher than 50 GPa are not considered in the analysis as it is assumed to be unreacted cement clinker grains (Nemecek, 2009).

The results indicated that the incorporation of nano-SiO_2 in HVFA cement pastes increased the amounts of both low and high density CSH. The results also indicated that the CH is also reduced in both HVFA pastes due to the addition of 2% nano-SiO_2 as shown in Figs. 5 and 6. In addition, it was observed that the probability of elastic modulus of loose-pack CSH, which represents the porous phase is also reduced in the HVFA pastes containing nano-SiO_2 (Figs. 5 and 6). These results confirmed the ability of nano-SiO_2 in reducing the porosity by filling the pores between the CSH gels through generating more low-density-CSH and high-density-CSH products. The effects of 1% nano-$CaCO_3$ on the indentation modulus and hardness of HVFA pastes are shown in Figs. 7 and 8. It was observed that the peak of the distribution of the indentation modulus of loose-pack CSH (porous phase) in FA40 mix was significantly reduced due to the addition of 1% nano-$CaCO_3$. However, no such improvement was observed in FA60 mix. The peaks of the probability plot of the elastic modulus, which corresponds to the low and high-density CSH gel for FA39NC1 and FA59NC1 were found to be in the range of 10-30 GPa and 20-35 GPa, respectively.

The values of elastic modulus and hardness for individual hydrated phase in HVFA cement pastes containing nano-SiO_2 and nano-$CaCO_3$ extracted from model fits are summarised in Table 3. Volume fractions of different hydration phases of HVFA pastes are also shown in the same table. As can be seen in this table, the relative percentage of low-density -CSH and high-density-CSH of HVFA cement paste containing 2% nano-SiO_2 were 37.5% and 15.9%, respectively for mix FA38NS2, whereas these values for the mix FA58NS2 were 37.4% and 23.3%%, respectively. The results were higher than the relative volume fractions of low-density-CSH and high-density-CSH in control HVFA pastes, which were about 17.3% and 16.4%%, respectively for the mix FA40 and 36% and 15.8%%, respectively for the mix FA60. The beneficial effect of addition of 2% nano-SiO_2 in HVFA pastes can also be seen where the volume fraction of loose packed CSH of FA40 and FA60 is reduced by 33% and 17%, respectively. Similarly, the volume fraction of CH of FA40 and FA60 is also reduced by 20% and 26%, respectively. It can be also seen in Table 3 that the total volume fraction of high- and low-density CSH in FA39NC1 increased by about 71% while a marginal increase is observed in FA59NC1. Despite this observation, the overall results suggested that the addition of both nano-SiO_2 and nano-$CaCO_3$ modified the HVFA cement paste properties by filling the pores in the CSH gels and decreasing the porosity.

The nanoindentation results showed the evidence of pozzolanic reaction in HVFA pastes containing nano-SiO_2, where the total volume of loose-packed-CSH is decreased from 54.4% to 36.9% and from 34.2% to 28.6% due to addition of 2% nano-SiO_2 in FA40 and FA60 pastes, respectively. At the same time the volume of CH in FA38NS2 and FA58NS2 pastes is decreased by about 20% and 26%, respectively due to addition of 2% nano-SiO_2. These are the clear evidence of pozzolanic reaction by nano-SiO_2 in HVFA pastes, which is consistent with other microstructural analysis results presented in other sections. In the case of HVFA paste containing 1% nano-$CaCO_3$ (FA39NC1) the loose-packed CSH is decreased from 54.4% to 26.7%, however no significant improvement is observed in the case of FA59NC1. Interestingly the addition of 1% nano-$CaCO_3$ increased the volume of CH in both HVFA pastes. One possible explanation of this behaviour in HVFA pastes is the seeding effect of nano-$CaCO_3$ particles on the nucleation of CSH. The nucleation of CSH is accelerated by the presence of nano-$CaCO_3$ particles on the surface of OPC and fly ash grains as evidenced by other researchers e.g. in (Sato and Beaudoin, 2011; Kawashima et al, 2014; Sato, and Diallo, 2010). There is also experimental evidence reported by many researchers e.g. in (Pera et al., 2004; de Weerdt et al., 2011; Larsen, 1961) that the calcium carbonate accelerates the hydration of tri-calcium silicate and modifies the CSH. This means that more CH is also produced due to hydration reaction of tri-calcium silicate in the matrix. It is also reported that the calcium carbonate acts as crystallization nuclei and thereby increase the crystallization rate of CH and consequently also the rate of cement hydration. This also agrees with the observed results in HVFA paste containing nano-$CaCO_3$. The higher CH in HVFA pastes containing nano-$CaCO_3$ than those containing nano-SiO_2 is also believed to be due to curing as all pastes were cured for only 28 days. After long curing the amount of CH in HVFA paste containing nano-$CaCO_3$ is expected to be reduced through pozzolanic reaction of fly ash present in the system. Thus, more research on the effect of long-term curing, their types as well as the effect of different water/binder ratios on the hydration of HVFA paste containing both nanoparticles are required to better understand the role of nanoparticles on the microstructure of HVFA paste.

3.3 X-ray diffraction (XRD) analysis

XRD patterns of HVFA pastes containing 38% fly ash+ 2% nano-SiO_2 and 58% fly ash+2% nano-SiO_2, respectively are shown in Figs. 9 and 10. The XRD patterns of control HVFA pastes containing 40% and 60% fly ash are also shown in the same Figs. for comparison. The highest CH peak with intensity counts of about 4800 and slightly higher than 5000 was observed at 2-theta angle of 18.05^0 in the HVFA pastes containing 40% and 60% fly ash,

respectively. The effects of adding 2% nano-SiO_2 in the above pastes in terms of consumption of CH can also be seen in the above Figs. It can be seen that the highest CH peak at the same angle in HVFA pastes containing 38% and 58% fly ash pastes is reduced by about 10% and 30%, respectively due to the addition of 2% nano-SiO_2. Larsen (1961) recognized that the CH concentration is inversely related to C-S-H production. If C-S-H is increased, less CH is available for diffracting X-rays (Belkowitz, and Armentrout, 2010). The reduction of CH in HVFA cement pastes containing nano-SiO_2 indicated the formation of more CSH in the system. Figs. 11 and 12 show the XRD patterns of HVFA cement pastes containing 39% fly ash+1% nano-$CaCO_3$ and 59% fly ash +1% nano-$CaCO_3$, respectively. The XRD patterns of control HVFA pastes containing 40% and 60% fly ash are also shown in the same Figs. for comparison. In HVFA cement paste containing 40% fly ash the intensity peak of CH was 4800 counts which reduced to about 4200 at $2\theta = 18.05°$ due to the addition of 1% nano-$CaCO_3$. In HVFA cement paste containing 60% fly ash the intensity peak of CH was 5000 counts which reduced to 3500 counts at $2\theta = 18.05°$.

3.4 DTA/TGA analysis

The results of DTA/TGA on HVFA cement pastes containing 2% nano-SiO_2 and 1% nano-$CaCO_3$ are shown in Figs. 13-16. DTA results showed two major endothermic peaks at 103°C and 462°C, corresponding to the dehydration of calcium silicate hydrate (CSH)/ettringite (AFt) and calcium hydroxide (CH), respectively (Vedalakshmi et al., 2003; Ukrainczyk et al., 2006). In Figs. 13-16, smaller broad peaks can be seen within the temperature range of 428-495°C indicating the less intensive CH in HVFA cement pastes containing nano-SiO_2 and nano-$CaCO_3$. The TGA curves also showed similar trend to explain that nanoparticles participated in the hydration process of the system. The weight loss due to the dehydroxylation of CH can be observed at temperature range between 400 and 500°C. The estimation of the content of CH is calculated based on Taylor formula as discussed earlier in Equation (7). It can be seen in Fig. 17 that the CH decreased in HVFA pastes due to the addition of nano-SiO_2, except the FA58NS2 paste where slight increase in CH is observed. It can also be seen that the presence of 1% nano-$CaCO_3$ reduced the CH content of pastes for both fly ash contents. This could be due to the reactivity of both nanoparticles in HVFA cement paste and the consumption of CH by the pozzolanic reaction. The reduction in CH content also confirmed the results obtained in nanoindentation studies in HVFA paste containing 2% nano-SiO_2, where the volume fraction of CH phases is reduced in both HVFA contents.

3.5 Mercury intrusion porosimetry (MIP)

The effects of nano-SiO_2 and nano-$CaCO_3$ on the porosity of HVFA cement paste are shown in Figs. 18 and 19. It shows the relationship between cumulative pore volume and pore diameter in the range of 0.01 to 100µm. Zhang and Islam (2012) classified the pores in cement pastes as large capillary pores, medium capillary pores and gel pores which are in the range of 10-0.05µm, 0.05-0.01 µm and <0.01µm, respectively. Gel pores form a part of CSH and are considered as micro pores. They are not active in water permeability and do not influence the strength. However, they influence shrinkage and creep of the concrete. The capillary pores are partially and completely filled with water and reduce as hydration continues. However, they affect the strength and durability of concrete (Brandt, 1995).

From Fig. 18 it can be seen that the total pore volume particularly the capillary pores of HVFA cement pastes is significantly reduced due to the addition of 2% nano-SiO_2. The paste with 60% fly ash had a coarser pore structure with a total porosity of about 0.61 cc/g and initial pore entry diameter of about 2 µm. On the other hand, in paste FA40, the total porosity and the initial pore entry diameter of about 0.39 cc/g and 1.0 µm, respectively. The higher capillary pores of HVFA pastes can be attributed to the less cement and hence, less CSH formed during hydration reaction and slow pozzolanic reaction of fly ash in the concrete. Similar higher porosity of HVFA mortar than OPC mortar is also observed by others (Ahmed et al., 2007). On the other hand, due to large surface area and higher fineness of nano-SiO_2 than the fly ash, more CSH gels are formed in HVFA pastes containing nano-SiO_2, which contributed to the reduction in capillary pores and gel pores. The results in Fig. 19 showed that the cumulative pore volume of HVFA paste containing 40% fly ash is reduced from 0.61 to 0.32 cc/g and that containing 60% fly ash is reduced from 0.39 to 0.28 cc/g due to addition of 2% nano-SiO_2. Similarly, the initial pore entry diameter of FA60 and FA40 pastes decreased from about 2 µm to 0.3 µm and from 1 µm to 0.2 µm, respectively due to the addition of 2% nano-SiO_2.

The effects of nano-$CaCO_3$ on the porosity of HVFA cement pastes are shown in Fig. 19. There was a notable reduction in pore concentration indicating the presence of nano-$CaCO_3$ is beneficial for pore modification. The result showed that the cumulative pore volume in HVFA pastes is reduced significantly due to addition of 1% nano-$CaCO_3$. While the total porosity of FA40 and FA60 are 0.39 and 0.61 cc/g, respectively, it reduced to 0.20 and 0.32 cc/g in the FA39NC1 and FA59NC1 paste samples, respectively. Both capillary and gel pores are reduced significantly by the addition of nano-$CaCO_3$ in HVFA system. The results also showed that the initial pore entry diameter is significantly reduced from 2 µm to 0.7 µm in

346 FA40 paste and from 1 µm to 0.2 µm in FA60 paste due to the addition of 1% nano-$CaCO_3$.
347 These results confirmed a dense microstructure of the HVFA pastes containing nano-SiO_2 and
348 nano-$CaCO_3$, which are in agreement with the results of XRD, DTA/TGA and
349 nanoindentation.

350

351 **4. Conclusions**

352 Based on the results obtained in this study the following conclusions can be made:

353 (i) Nanoindentation results indicated that the incorporation of nano-SiO_2 at 2% and nano-
354 $CaCO_3$ at 1% in high volume fly ash cement pastes containing 40% and 60% fly ash
355 reduced the volume fractions of loose packed CSH and increased the low density CSH
356 except the mix FA59NC1 where slight increase and decrease, respectively is observed.
357 Nanoindentation results also show increase in the volume fractions of high density
358 CSH gel in all mixes except in FA38NS2 where no change is observed. The
359 nanoindentation results also show that the volume fraction of CH is reduced in HVFA
360 mixes due to addition of nano-SiO_2, whereas an opposite trend is observed in the case
361 of HVFA containing nano-$CaCO_3$. The latter is believed to be due to the accelerated
362 reaction of tri-calcium silicate due to the presence of nano-CaCO3, which ultimately
363 increased the CH content. The slow pozzolanic reaction of fly ash is also believed to
364 be the reason for high CH content in HVFA pastes containing nano-CaCO3.

365 (ii) XRD revealed that the addition of 2% nano-SiO_2 and 1% nano-$CaCO_3$ in HVFA
366 cement paste increased the consumption of CH and, hence, the formations of CSH gel.
367 However, this trend is deviated in FA39NC1 mix where no significant reduction in
368 CH is noticed. The DTA/TGA also confirmed the findings of XRD results showing
369 the reactivity of nano-SiO_2 and nano-$CaCO_3$ in reducing the CH content, with only
370 exception in the FA58NS2 mix.

371 (iii) MIP results confirmed the ability of nano-SiO_2 and nano-$CaCO_3$ in reducing the total
372 capillary pores and pore diameter of HVFA cement paste. The results confirmed a
373 dense microstructure of the HVFA cement paste with the addition of 2% nano-SiO_2
374 and 1% nano-$CaCO_3$.

375 The improved microstructure of HVFA pastes due to addition of nano-SiO_2 and nano-
376 $CaCO_3$ observed through the nano and microstructural analysis confirmed that the
377 mechanical and durability properties of sustainable high volume fly ash concretes can be
378 improved, which will contribute significantly in the infrastructure sustainability.

379

References

- Ahmed, **S.F.U**., Maalej, M. and Paramasivam, P, (2007) Flexural responses of hybrid steel-polyethylene fiber reinforced cement composites containing high volume fly ash. *Journal of Construction and Building Materials.* Vol. 21, No. 5, pp.1088-1097.
- Belkowitz, J.S., and Armentrout, D., (2010) "An investigation of nano silica in the cement hydration process". *2010 Concrete Sustainability Conference,* National Ready Mixed Concrete Association.
- Bendapudi, S.C.K., (2011) "Contribution of fly ash to the properties of mortar and concrete". *International Journal of earth Sciences and Engineering*, Vol. 04, No 06 SPL, pp 1017-1023.
- Brandt, M,A., (1995). "Cement-based composites-Materials, mechanical properties and performance". Second edition. Taylor and Francis Group. ISBN: 0-203-88903-7.
- Constantinides, G. and Ulm, F.-J.: 'The effect of two types of C–S–H on the elasticity of cement-based materials: results from nanoindentation and micromechanical modeling,' Cem Concr Res., 2004, 34, pp. 67–80.
- De Weerdt, K., Kjellsen, K.O., Sellevoid, E.J. and Justnes, J., (2011) "Synergy between fly ash and lime stone powder in ternary cements". *Cement and Concrete Research,* 41, 279-291.
- de Weerdt, K., Kjellsen, K.O., Sellevold, E. and Justnes, H. (2011) Synergy between fly ash and limestone powder in ternary cements. Cement and concrete composites, Vol.33:30-38.
- Hou, P, Kawashima, S, Wang, K, Corr, D, Qian, J, Shah, S., (2013) "Effects of colloidal nanosilica on rheological and mechanical properties of fly ash-cement mortar". *Cement and Concrete Composite,* Vol, 35, pp, 12-22.
- Kawashima, S., Seo, J.W.T., Corr, D., Hersam, M.C. and Shah, S.P. (2014) Dispersion of CaCO3 nanoparticles by sonication and surfactant treatment for application in fly ash system. Materials and structures. 47:1011-1023.
- Larsen, G., (1961) "Microscopic point measuring: a quantitative petrographic method of determining the Ca(OH)2 content of the cement paste of concrete". *Magazine of Concrete Research*, 13(38), 71-76.
- Li, H., Xiao, H., Yuan, J., & Ou, J., (2004) "Microstructure of cement mortar with nano-particles". *Composites: Part B, 35,* 185-189.
- Malhotra, V.M. and Mehta, P.K., (2002) *"High-performance, high-volume fly ash concrete: materials, mixture proportioning, properties, construction practice, and case histories"*. ISBN: 0-9731507-0-X.
- Malvar, L.J., and Lenke, L.R., (2006) "Efficiency of Fly Ash in mitigating alkali silica reaction based on chemical composition", *ACI Material Journal*, Vol. 103, No.5, September-October 2006, pp. 319-326.
- Matschei, T., Lothenbach, B. and Glasser, F.P. (2007) The role of calcium carbonate in cement hydration. *Cement and concrete research*. 37:551-558.
- Mehta, P.K., (2004) "High performance, high volume fly ash concrete for sustainable development". *Proceedings of the International Workshop on Sustainable Development and Concrete Technology,* Iowa State University, USA, ISBN 0-9652310-7-0.
- Němeček, J. (2009). Creep effects in nanoindentation of hydrated phases of cement pastes, Materials Characterization 60 (9), pp. 1028–1034.
- Pera, J., Husson, S., and Guilhot, B., (1999) "Influence of finely ground limestone on cement hydration". *Cement and Concrete Composites,* 21, 99-105.

- Sato, T. and Beaudoin, J.J., (2011) "Effect of nano-$CaCO_3$ on hydration of cement containing supplementary cementitious materials", *Advances in Cement Research,* Vol.23, pp. 33-43.
- Sato, T. and Diallo, F. (2010) Seeding effect of nano-CaCO3 on the hydration of tricalcium silicate. Journal of transportation research board. Vol. 2141:61-67.
- Shaikh, F.U.A. and Supit, S.W.M. (2015) Compressive strength and durability properties of high volume fly ash concretes containing ultrafine fly ash. *Construction and building materials. (*DOI:10.1016/j.conbuildmat.2015.02.068*)*
- Shaikh, F.U.A. and Supit, W.M.S. (2014) Mechanical and durability properties of high volume fly ash (HVFA) concrete containing calcium carbonate ($CaCO_3$) nanoparticles. *Construction and building materials.* Vol. 70:309-321.
- Shaikh, F.U.A., Supit, S. and Sarker, P. (2014) A study on the effect of nano silica on compressive strength of high volume fly ash mortar and concrete, *Materials and design.* Vol.60: 433-442.
- Shi, C, and Shao, Y., (2002) "What is the most efficient way to activate the reactivity of fly ashes". *2nd Material Specialty Conference of the Canadian Society for Civil Engineering,* June 5-8, 2002.
- Siddique, R., (2004) "Performance characteristics of high-volume Class F fly ash concrete". *Cement and Concrete Research,* 34(3): 487-493.
- Sorelli, L., Constantinides, G., Ulm, F.J. and Toutlemonde, F.: 'The nano-mechanical signature of ultra high performance concrete by statistical nanoindentation techniques,' Cem Concr Res., 2008, 38(12), pp. 1447–1456.
- Supit, W.M.S. and Shaikh, F.U.A. (2014a) Effect of nano-$CaCO_3$ on compressive strength development of high volume fly ash mortars and concretes, *Journal of Advanced Concrete Technology.* Vol. 12:178-186.
- Supit, W.M.S. and Shaikh, F.U.A. (2014b) Durability properties of high volume fly ash concrete containing nano silica. *Materials and structures. (*DOI 10.1617/s11527-014-0329-0*)*
- Supit, W.M.S., Shaikh, F.U.A. and Sarker, P. K. (2014) Effect of Ultrafine Fly Ash on Mechanical Properties of High Volume Fly Ash Mortar, *Construction & Building Materials. Vol. 51:278-286.*
- Tahir, M.A., and Sabir, M., (2005) "A study on durability of fly ash-cement mortars", *30th conference on "Our world in concrete and structure": 23-24 August 2005, Singapore,* article online Id: 100030019.
- Taylor, H.F.W., (1990) "Cement chemistry", *Academic Press Limited,* London.
- Vandamme, M., Ulm, F.J. and Fonollosa, P.: 'Nanogranular packing of C–S–H at substochiometric conditions,' Cem Concr Res., 2010, 40(1), pp. 14–26.
- Zhang, M.H. and Islam, J., (2012) "Use of nano-silica to reduce setting time and increase early strength of concretes with high volume fly ash or slag". *Construction and Building Materials*, Vol. 29, pp.573-580.
- Zhu, W., Hughes, J.J., Bicanic, N. and Pearce, C.J.: 'Nanoindentation mapping of mechanical properties of cement paste and natural rocks,' Materials Characterization, 2007, 58, pp. 1189-1198.
- Vedalakshmi, R., Sundara Raj, A., Srinivasan, S. and Ganesh babu, K. (2003) Quantification of hydrated cement products of blended cements in low and medium strength concrete using TG and DTA technique. Thermochimica Acta, 407:49-60.
- Ukrainczyk, N., Ukrainczyk, M., Sipusic, J. and Matusinovic, T. (2006). XRD and TGA investigation of bydrated cement paste degradation. In Conference on materials, processes, friction and wear, MATRIB'06, Vela Luka, 22-24 June, 2006.

480 **Table 1:** Physical properties and chemical composition of materials used
481

Chemical composition				
Oxides (%)	OPC	Fly ash	Nano-SiO_2	Nano-$CaCO_3$
SiO_2	20.2	51.80	99	-
Al_2O_3	4.9	26.40	-	-
Fe_2O_3	2.8	13.20	-	0.02
CaO	63.9	1.61	-	97.8
MgO	2.0	1.17	-	0.5
MnO	-	0.10	-	-
K_2O	-	0.68	-	-
Na_2O	-	0.31	-	-
P_2O_5	-	1.39	-	-
TiO_2	-	1.44	-	-
SO_3	2.4	0.21	-	-
Physical Properties				
Particle size	25-40% ≤ 7µm	40% of 10 µm	25 nm	15 – 40 nm
Specific gravity	2.7 to 3.2	2.6	2.2 to 2.6	-
Surface area (m^2/g)	-	-	160	40
Loss on ignition (%)	2.4	0.5	-	-

482

483 **Table 2:** Mix proportions

Mix ID	Cement	Fly ash	Nano-SiO_2	Nano-$CaCO_3$	Water
	(kg/m^3)				
FA40	240	160	-	-	160
FA60	160	240	-	-	160
FA38NS2	240	152	8	-	160
FA58NS2	160	232	8	-	160
FA39NC1	240	156	-	4	160
FA59NC1	160	236	-	4	160

484
485
486
487
488
489
490
491 **Table 3:** Elastic modulus and hardness values extracted from model fits for individual
492 hydrated phases in of HVFA cement pastes containing Nano-SiO_2 and Nano-$CaCO_3$
493

MIX	Phases	Elastic modulus (GPa)	Hardness (GPa)	Volume fraction (%)
FA40	Loose-packed CSH	10.03	0.24	54.4
	Low density CSH	21.04	0.50	17.3
	High density CSH	30.11	0.88	16.4
	CH	41.30	1.30	11.9
FA60	Loose-packed CSH	11.02	0.22	34.2

	Low density CSH	20.00	0.54	36.0
	High density CSH	30.31	0.59	15.8
	CH	44.75	1.37	14.5
FA38NS2	Loose-packed CSH	8.00	0.18	36.9
	Low density CSH	14.25	0.35	37.5
	High density CSH	27.82	0.84	15.9
	CH	42.31	1.53	9.6
FA58NS2	Loose-packed CSH	7.56	0.15	28.6
	Low density CSH	14.15	0.35	37.4
	High density CSH	28.08	0.71	23.3
	CH	44.53	1.36	10.8
FA39NC1	Loose-packed CSH	14.34	0.38	26.7
	Low density CSH	20.82	0.66	36.9
	High density CSH	28.00	1.10	20.9
	CH	41.11	1.71	15.5
FA59NC1	Loose-packed CSH	8.19	0.15	36.1
	Low density CSH	19.20	0.50	28.8
	High density CSH	29.50	0.94	23.37
	CH	38.50	1.54	30.25

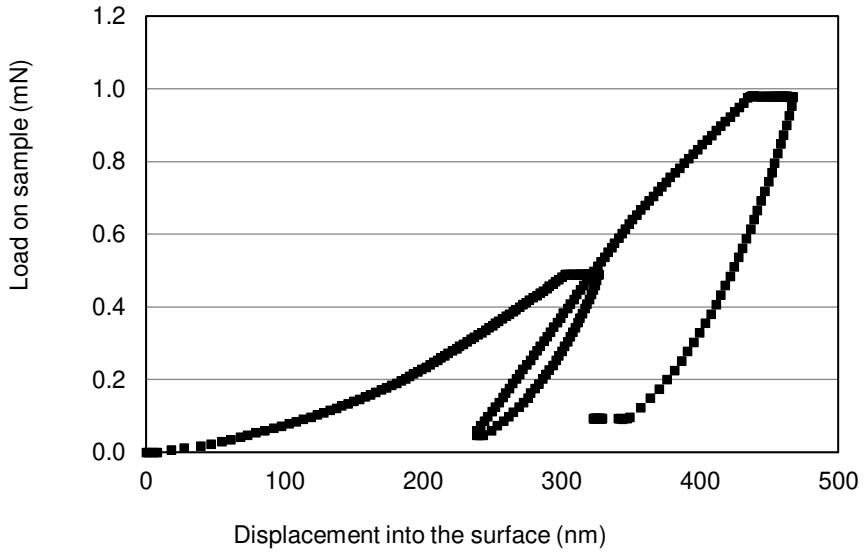

Fig. 1: Typical load-displacement curves in nanoindentation test

498

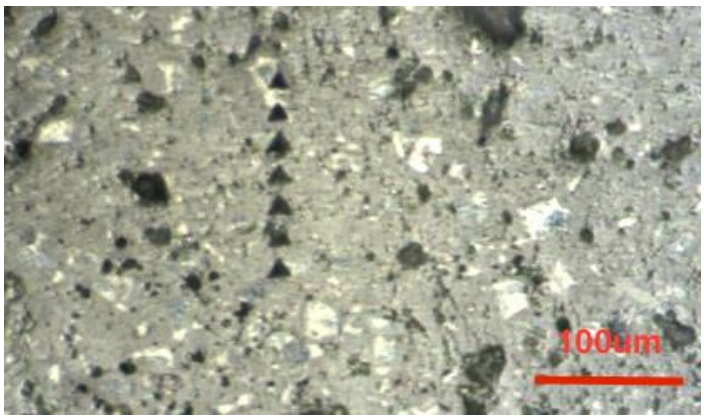

499 **Fig. 2:** A typical micrograph showing indents

500

501

502

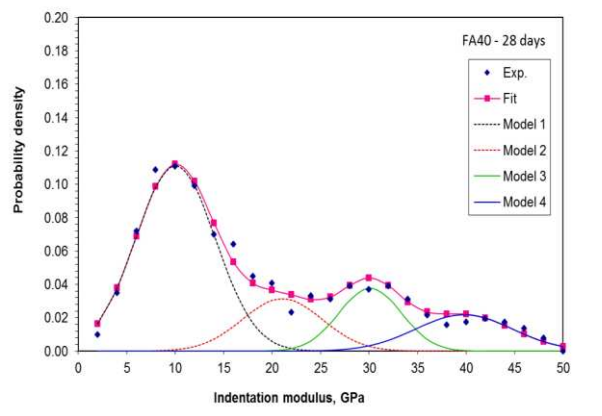

Fig. 3a: Probability density function (PDF) of modulus of FA40 paste

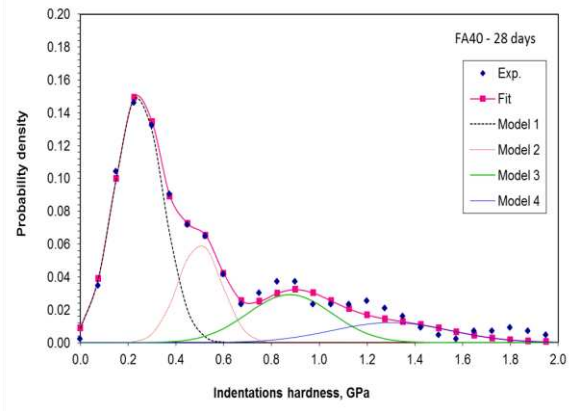

Fig. 3b: Probability density function (PDF) of hardness of FA40 paste

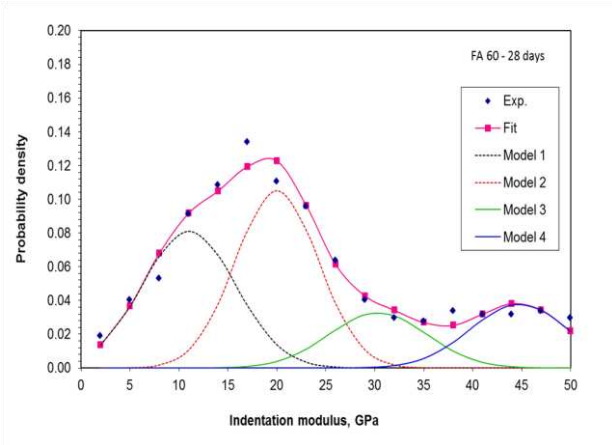

Fig. 4a: Probability density function (PDF) of

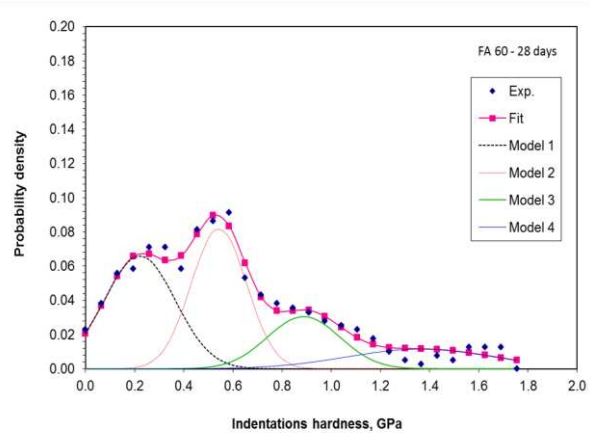

Fig. 4b: Probability density function (PDF)

modulus of FA60 paste	of hardness of FA60 paste
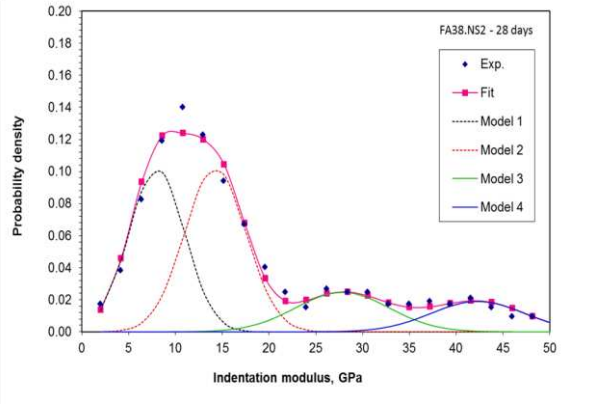	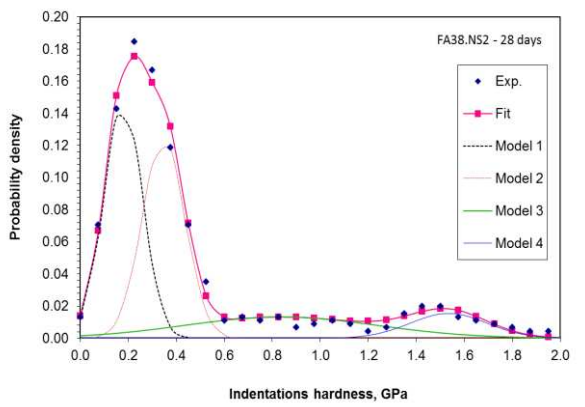
Fig. 5a Probability density function (PDF) of modulus of FA38NS2 paste	**Fig. 6b** Probability density function (PDF) of hardness of FA38NS2 paste

503

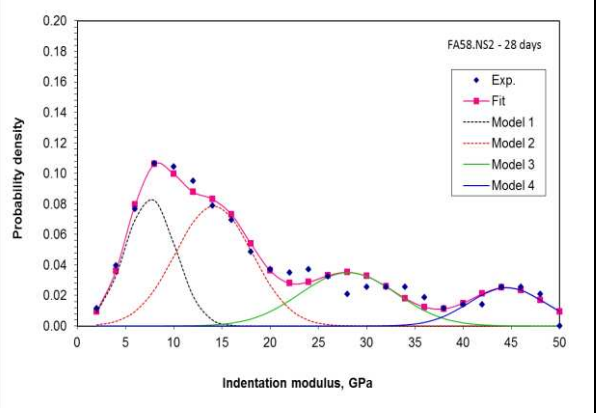	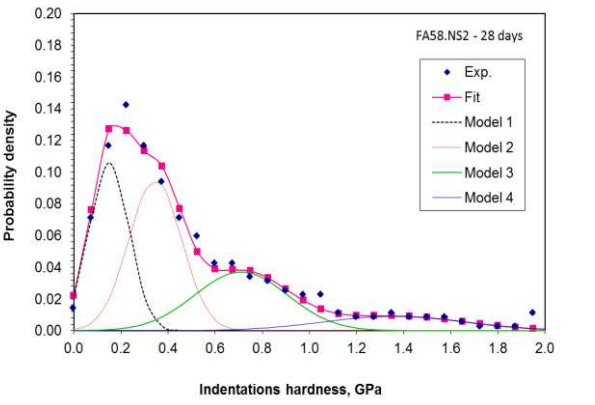
Fig. 6a Probability density function (PDF) of modulus of FA58NS2 paste	**Fig. 6b** Probability density function (PDF) of hardness of FA58NS2 paste
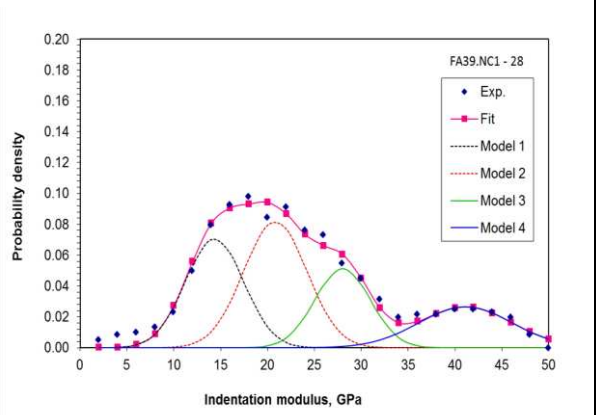	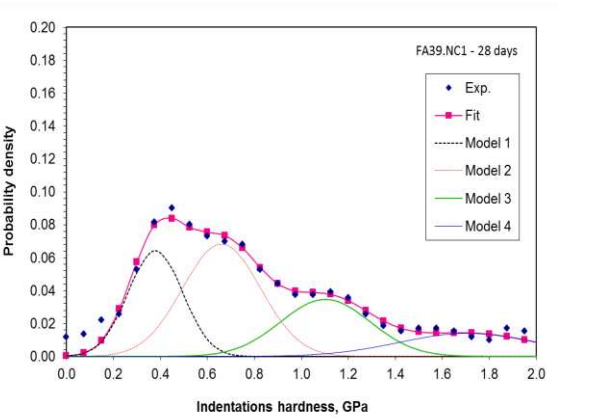
Fig. 7a Probability density function (PDF) of modulus of FA39NC1 paste	**Fig. 7b** Probability density function (PDF) of hardness of FA39NC1paste

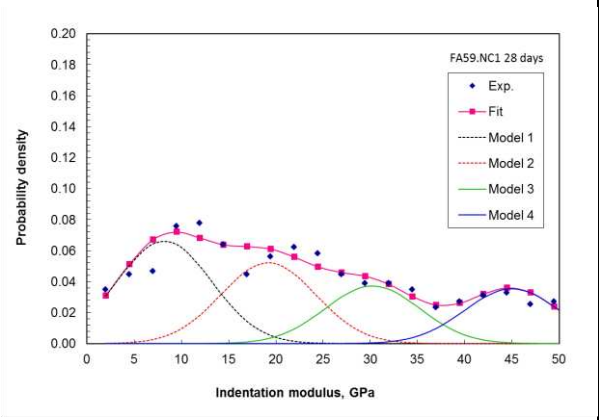

Fig. 8a Probability density function (PDF) of modulus of FA59NC1 paste

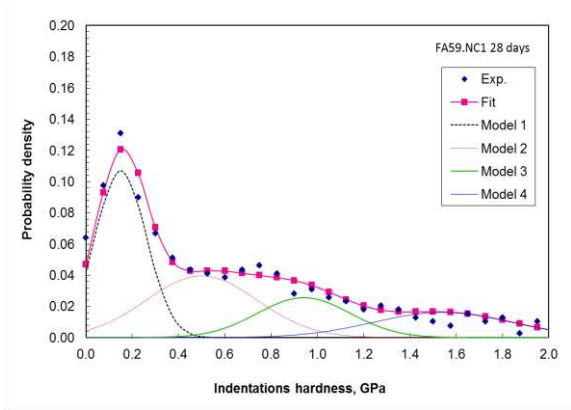

Fig. 8b Probability density function (PDF) of hardness of FA59NC1paste

504

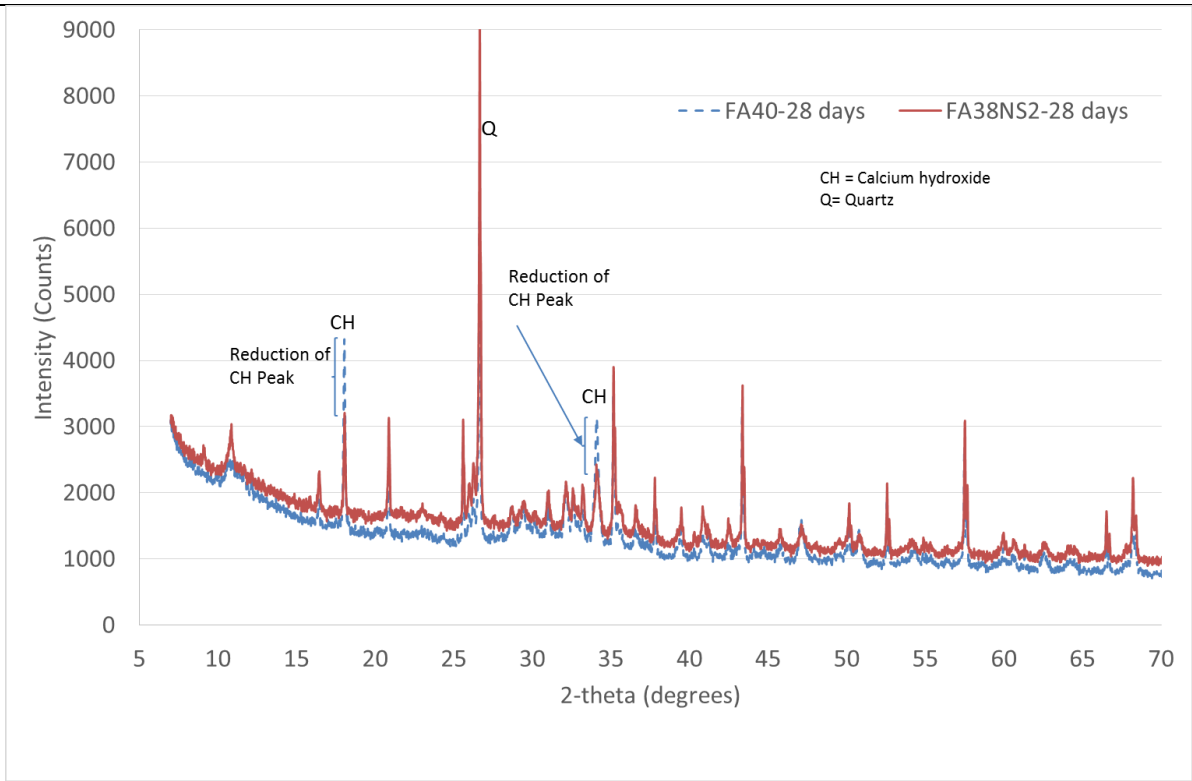

Fig. 9 XRD patterns of HVFA paste with 40% FA and 38%FA+2% nano-SiO_2

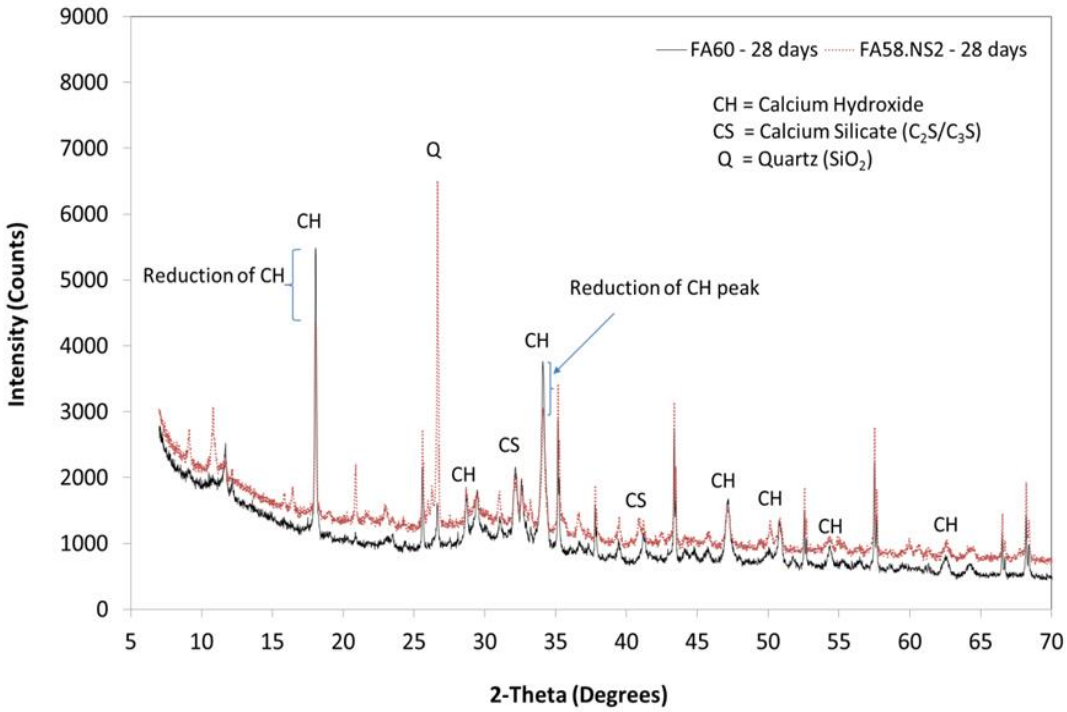

Fig.10 XRD patterns of HVFA paste with 60% FA and 58%FA+2% nano-SiO_2

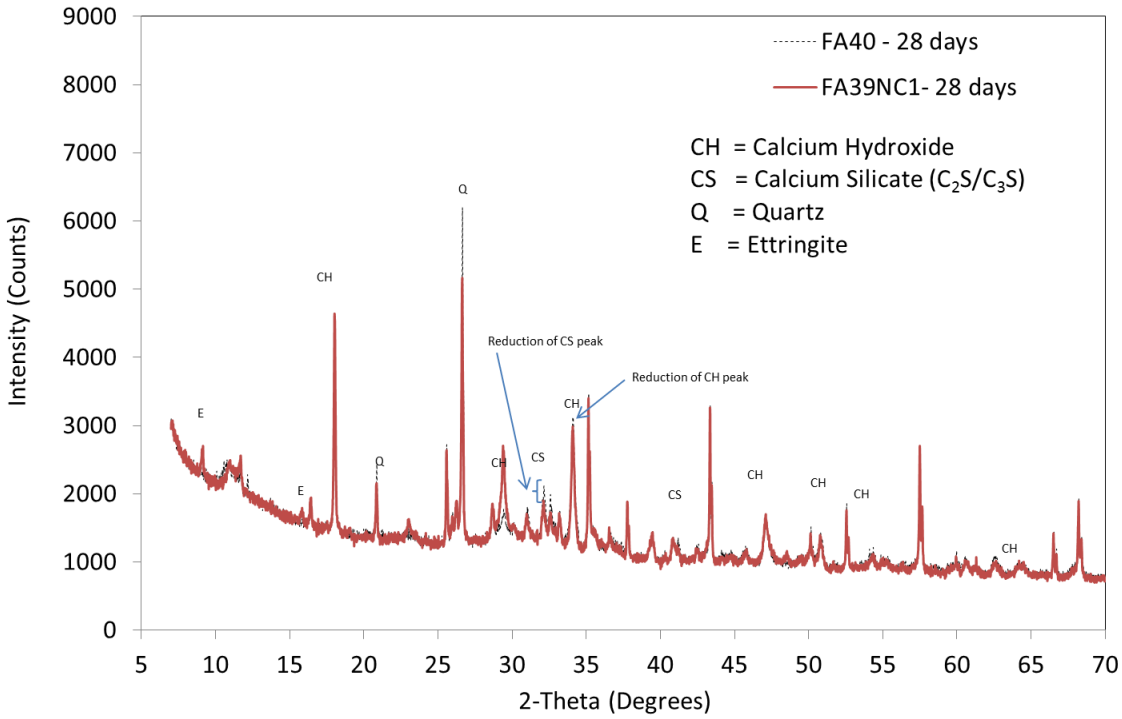

Fig. 11 XRD patterns of HVFA paste with 40% FA and 39%FA+1% nano-$CaCO_3$ (Shaikh and Supit, 2014)

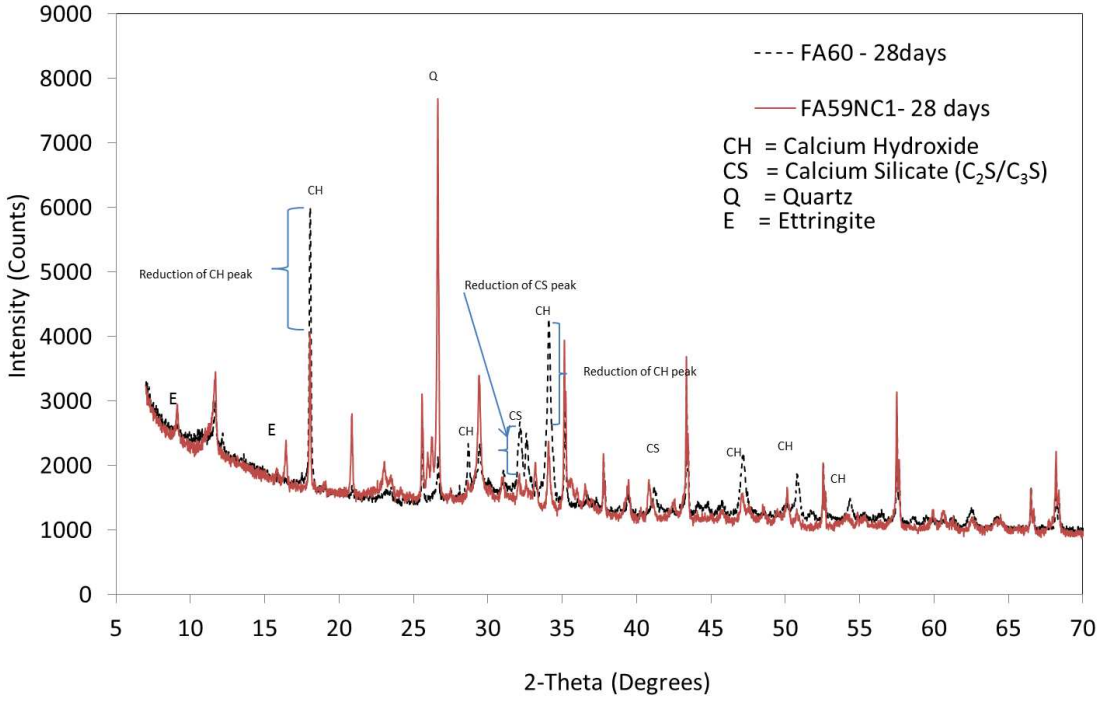

Fig. 12 XRD patterns of HVFA paste with 40% FA and 59%FA+1% nano-$CaCO_3$ (Shaikh and Supit, 2014)

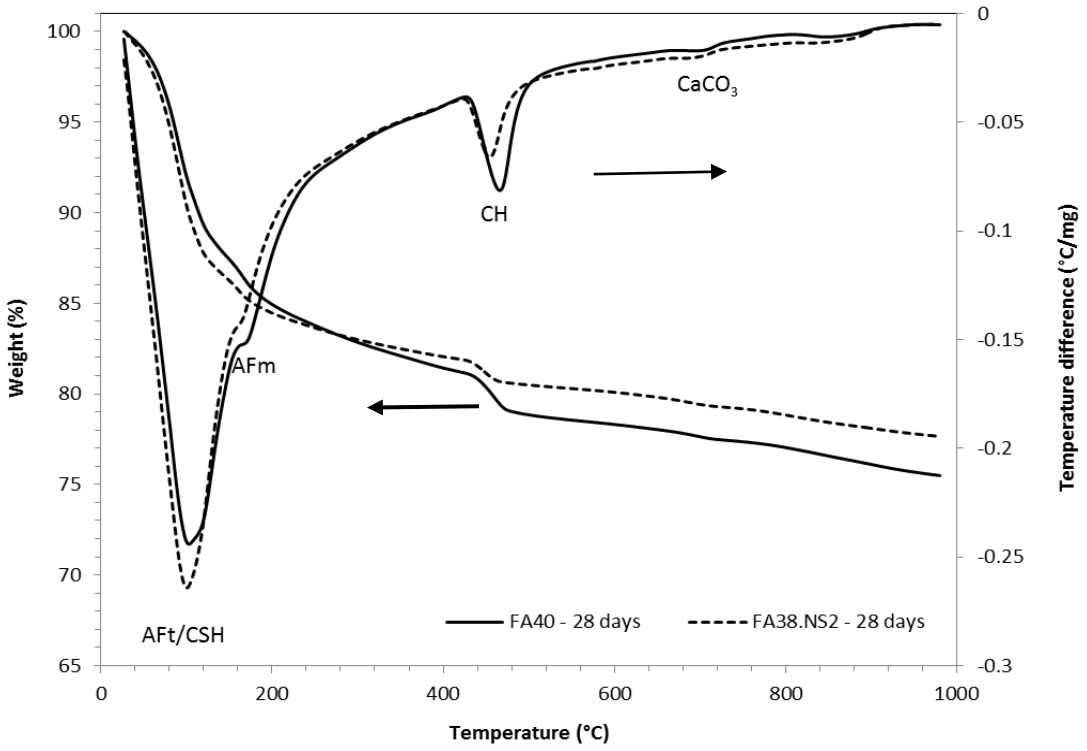

Fig. 13 DTA/TGA of HVFA paste with 40% FA and 38%FA+2% nano-SiO_2

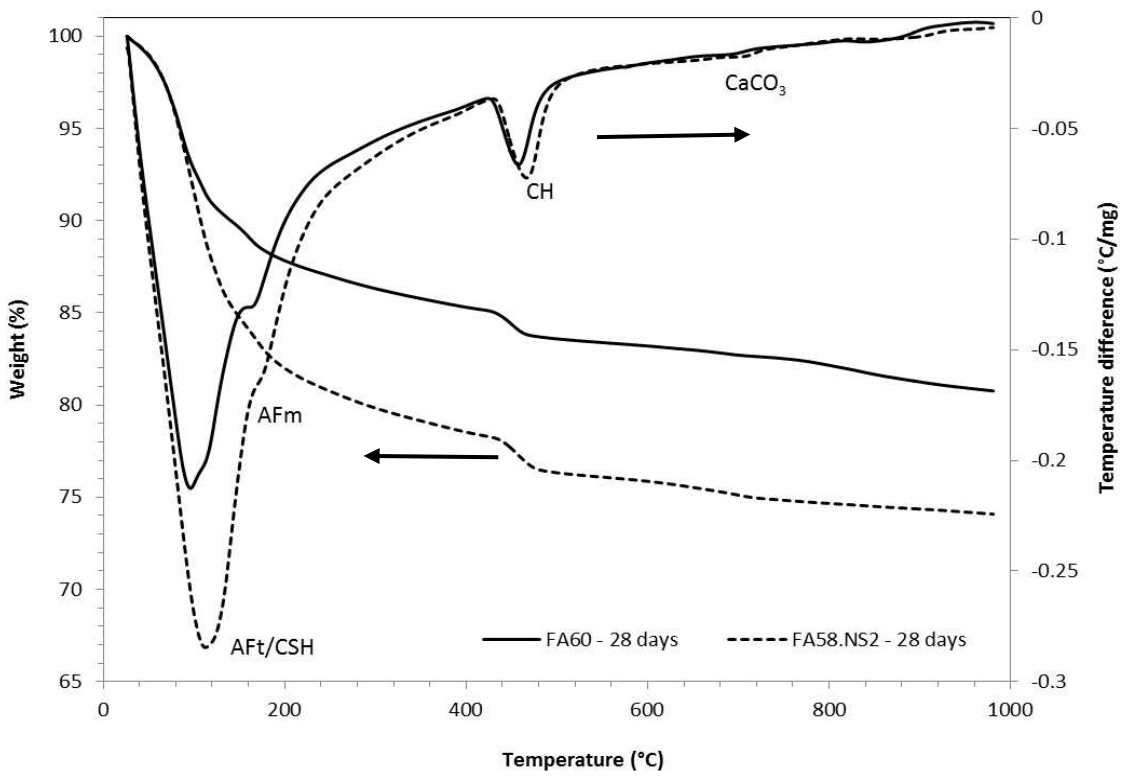

Fig. 14 DTA/TGA of HVFA paste with 60% FA and 58%FA+2% nano-SiO_2

506

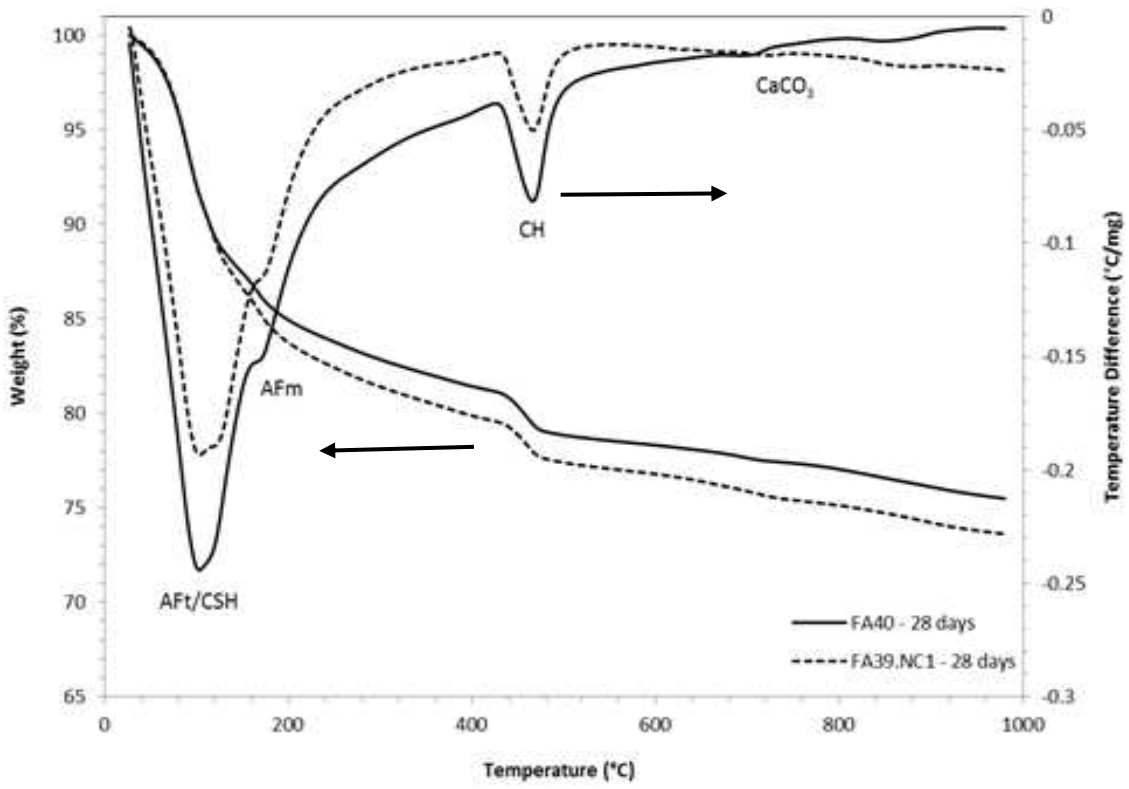

Fig. 15 DTA/TGA of HVFA paste with 40% FA and 39%FA+1% nano-$CaCO_3$ (Shaikh and Supit, 2014)

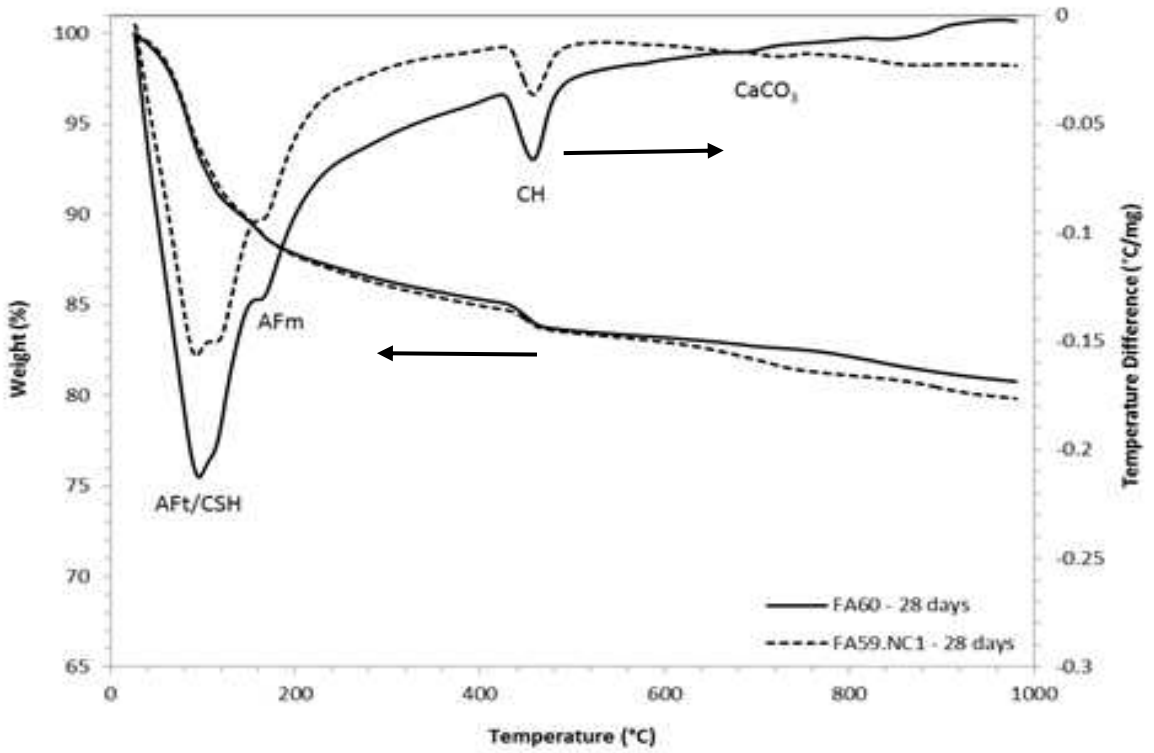

Fig. 16 DTA/TGA of HVFA paste with 60% FA and 59%FA+1% nano-$CaCO_3$ (Shaikh and Supit, 2014)

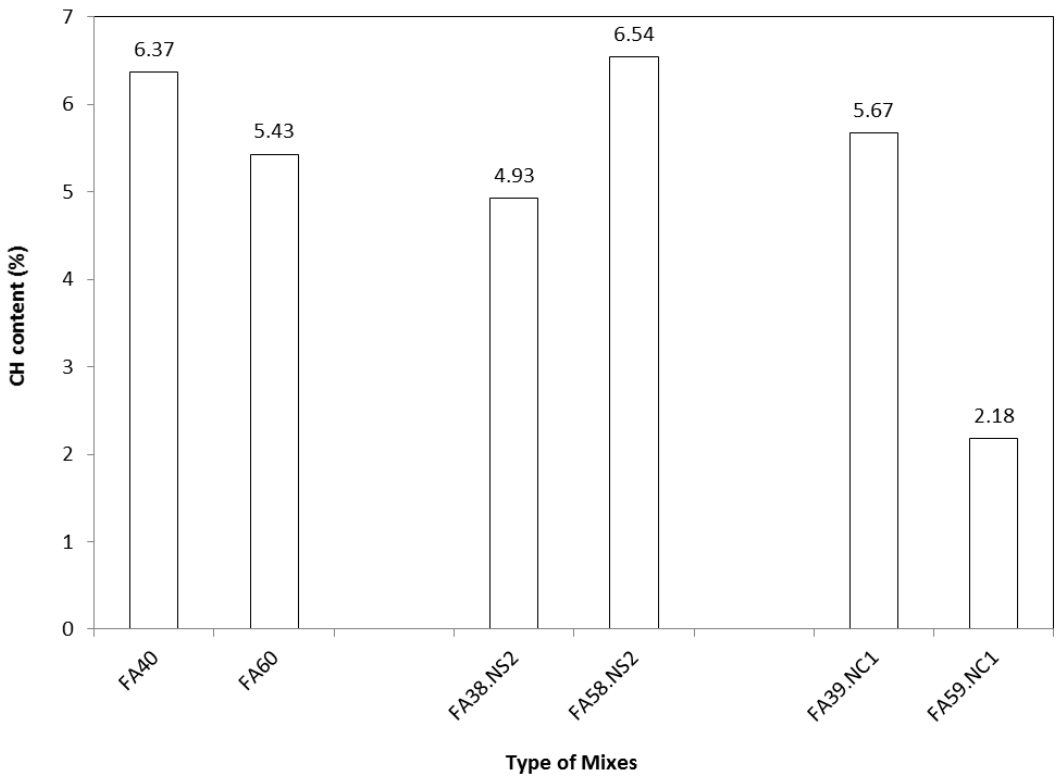

Fig. 17 CH content in HVFA pastes containing 2% nano-SiO_2 and 1% nano-$CaCO_3$

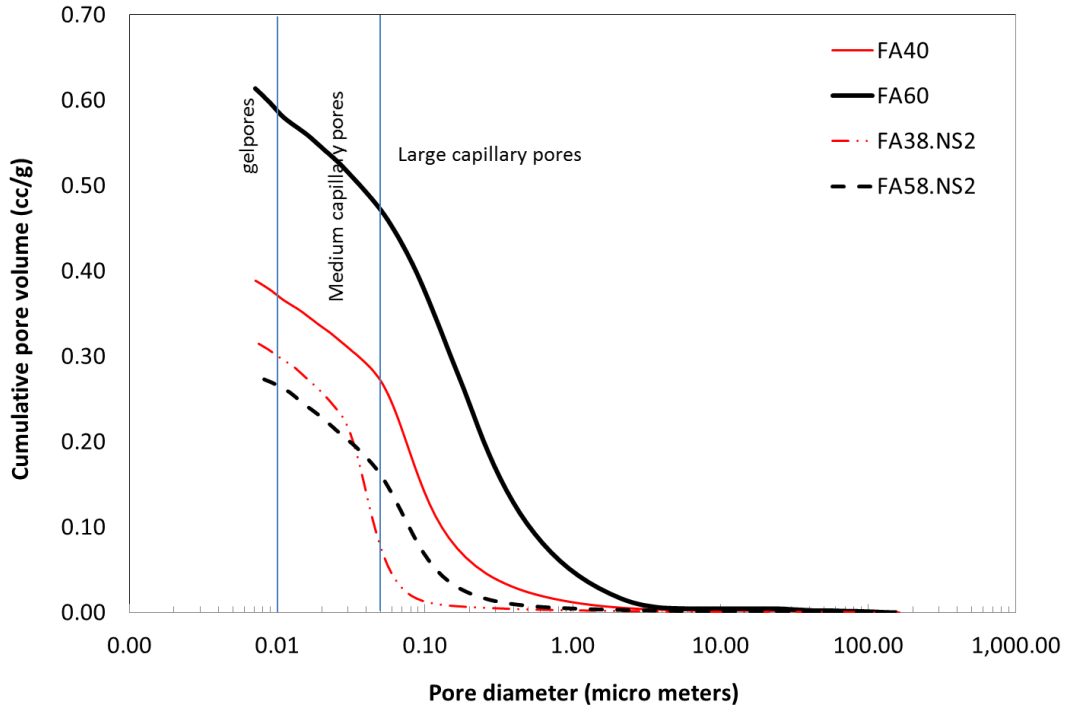

Fig. 18 Commutative pore volume of HVFA paste with and without 2% nano-SiO_2 [15]

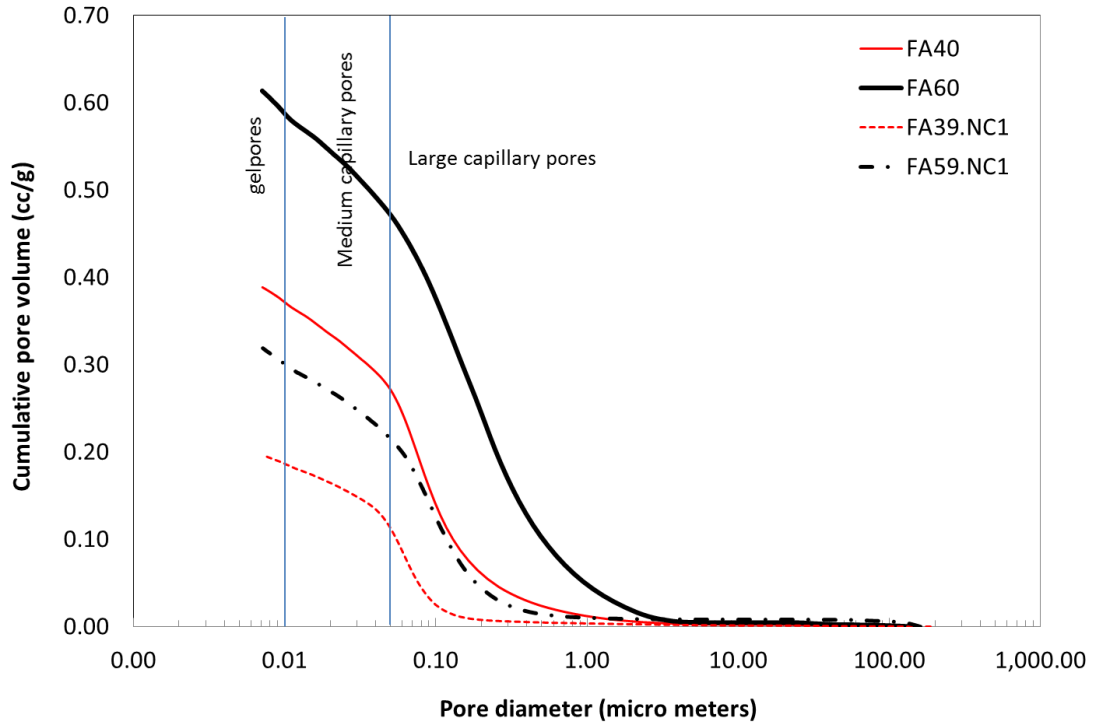

Fig. 19 Commutative pore volume of HVFA paste with and without 1% nano-$CaCO_3$ (Shaikh and Supit, 2014)

507